Earth and Planetary Science Letters 526 (2019) 115768

Contents lists available at ScienceDirect

Earth and Planetary Science Letters

www.elsevier.com/locate/epsl

Noachian climatic conditions on Mars inferred from valley network junction angles

Xuezhi Cang *, Wei Luo

Department of Geographic and Atmospheric Sciences, Northern Illinois University, DeKalb, IL, USA

ARTICLE INFO

Article history:
Received 1 April 2019
Received in revised form 29 July 2019
Accepted 10 August 2019
Available online xxxx
Editor: W.B. McKinnon

Keywords:
Mars
Noachian period
valley networks
junction angle
spatial analysis

ABSTRACT

Valley networks (VNs) on Mars offer convincing evidence for its past water activities. Previous research empirically and theoretically suggested that the geometry properties, such as junction angles, of streams on Earth formed under different climatic conditions are different. Thus the geometry properties of VNs can be used to infer the early Mars climatic conditions under which VNs were formed. The frequency distribution of junction angles is less influenced by the post-formational modification processes than valley density and cross-section and can be accurately extracted from low resolution data. We first analyzed the association between the junction angles and environmental factors on Earth. The results suggested that the climatic factors are stronger than or on par with the geologic factors in controlling junction angles and that climatic parameters Aridity Index (*AI*) and Mean Annual Precipitation (*MAP*) can be estimated from junction angles. We then applied the associations between terrestrial junction angle and climatic conditions to estimate the *AI* and *MAP* of Mars, considering the different solar radiation of the two planets. The spatial analysis of inferred climatic conditions showed that the Noachian Mars had an active global hydrological cycling and Mars was "warm" during the VNs' formation period. The duration of "warm" Mars is estimated by the ratio between the required water volume to form VNs and the runoff discharge derived from *MAP*. The range of "warm" period is from ~4.4 to ~77 million years. The results support the hypothesis that Mars was "episodically warm".

1. Introduction

Mars is currently a cold and dry planet, where liquid water could not exist stably on its surface. However, observations of valley networks (VNs) (Craddock and Howard, 2002), deltas (Di Achille and Hynek, 2010) and tsunami deposits (Rodriguez et al., 2016), among other evidences, suggest that Mars once had abundant liquid water during the Noachian period and the early Mars climate was "warm" enough to support liquid water (e.g., Craddock and Howard, 2002). Despite the many lines of geomorphic, geochemical, and geologic evidence that suggest an early warm Mars with abundant liquid water and an active hydrologic cycle (Luo et al., 2017), climate modelers have encountered difficulties in modeling such early warm and wet conditions with an above freezing temperature, mainly due to the Martian orbit and the faintness of the young Sun (e.g., Wordsworth et al., 2015). Since Mars is in an orbit farther away from the Sun, it receives only about 43% of the solar energy that Earth does and the Sun's luminosity 3.8 billion years ago (when most of the VNs were believed to be formed) was only ~75% of its present value (Gough, 1981). Wordsworth et al. (2015) compared the spatial distribution of modeled precipitation/ice accumulation with that of the VN density and found no correlation between them. In particular, the model predicted high precipitation in Arabia Terra, where low VN density was observed there. However, Davis et al. (2016), through detailed regional analysis and mapping of the orbiter images over Arabia Terra, showed evidence for extensive networks of inverted sinuous ridges, suggesting that previous VNs were eliminated by the resurfacing process; thus the evidence supports that the Mars had a more widespread precipitation and runoff than the modeled results from the climate model (Wordsworth et al., 2015). To reconcile the different views on early Mars climate, a number of alternative scenarios have been proposed. For example, the early climate of Mars could be warm and wet episodically because of brief and strong volcanic activities and associated outgassing of greenhouse gasses and aerosols (Halevy and Head, 2014); VNs could be formed by groundwater sapping associated with magma intrusion and hydrothermal activities, thus not requiring continuous warm and wet conditions (Gulick, 1998); VNs could be created during short-lived episodes of top-down melting of thick cold-

* Corresponding author.
E-mail address: xcang@niu.edu (X. Cang).

https://doi.org/10.1016/j.epsl.2019.115768
0012-821X/

based ice on the equatorial highlands (Wordsworth et al., 2015; Rosenberg et al., 2019).

The formation mechanism of Mars VNs is important in understanding the early Mars climate. The VNs' characteristics, such as cross-section shape, stream order, scaling relation, have been investigated quantitatively to derivate the climate condition of the Noachian period (Williams and Phillips, 2001; Hynek and Phillips, 2003; Penido et al., 2013). Their results support that Mars was "warm" enough to have liquid water flowing on the surface in the Noachian Mars; however, they did not answer the question about duration of "warm" period or the formation timescale of VNs, which directly relates to the long term climatic conditions. This question is answered by some research which applied the sediment transport models and the characteristic of VNs (depth, width, volume, etc.) to estimate the cumulative volume of water required to carve the VNs (Luo et al., 2017; Rosenberg et al., 2019) and the formation timescale of VNs (Hoke et al., 2011; Orofino et al., 2018). Due to the large uncertainties of derived VN characteristics data and the difference between models, the conclusions from these studies are different or even mutually exclusive. Hitherto, scientists are still debating on whether episodic warmth or non-precipitation dominated erosion can create the observed valley networks and trying to reconcile the geochemical and physical understanding of Mars with the geologic evidence of its watery past (Baker et al., 2015; Ehlmann et al., 2011; Wordsworth, 2016). Although the controversies still exist, the consensus between supporters of "Warm" Mars and "Cold" Mars is that abundant liquid water flowed on Mars in the Noachian period (Wordsworth et al., 2018; Ramirez and Craddock, 2018). Since characteristics used by earlier studies were likely influenced by the impact cratering and post-formation processes, it is necessary to choose a new characteristic of VNs, which is less influenced by the impact cratering and post-formation process, to estimate the climatic condition of the Noachian Mars.

The junction angle between two joining streams is one of the main characteristics of stream networks. Perron et al. (2012) revealed that the junction angle is not an outcome of random topology, but "an organized signature of erosional mechanics." To predict the junction angles, Horton (1932 and 1945) investigated the association between junction angles and other characteristics of basin, such as the slope/area ratio. Seybold et al. (2017) showed that the influence of aridity index to junction angles is stronger than the influence of elevation, slope and stream network concavity and suggested that the strength of coupling between groundwater and surface water processes influenced the size of junction angle.

Unlike other characteristics of streams, junction angle is less influenced by post-formational modification and can be accurately extracted even from low resolution data. For this reason, the junction angles of VNs on Mars were investigated in early research (Pieri, 1980). There is renewed interest in junction angles in recent literature that suggest that terrestrial stream junction angles and their frequency distribution reflect the relative dominance in the underlying channel forming processes and the climatic conditions under which the streams were formed (Hooshyar et al., 2017; Seybold et al., 2017). Seybold et al. (2018) extended the research area of Seybold et al. (2017) from the conterminous U.S to the global Earth surface, and analogized the junction angles of Earth and Mars to examine the paleoclimate in the Noachian period.

Seybold et al. (2017) analyzed millions of stream junctions throughout the conterminous U.S. and showed that mean junction angles by hydrologic units vary systematically with *AI* (aridity index = precipitation/potential evapotranspiration): $\sim 45^\circ$ in the driest places and $\sim 72^\circ$ in the humid areas. They interpreted the observed trend as due to the different geomorphic processes controlled by climate. The conclusion of Seybold et al. (2017) revealed that the junction angles are strongly associated with the climatic condition and can be utilized as an indicator of arid or humid climatic condition.

Based on the results of Seybold et al. (2017), Seybold et al. (2018) calculated the junction angles on the global Earth surface and found that the mean junction angles in each watershed increase with the aridity index. Then, Seybold et al. (2018) compared frequency of junction angles of Mars with that of Mars Desert Research Station (MDRS), which is an analog site located in the Upper Colorado-Dirty Devil basin in the arid southwestern United States, and found similarity between them, which confirms that the climatic environment of Noachian Mars is similar to that of the MDRS. Seybold et al. (2018) also compared the frequency of junction angles of Mars with the frequency of junction angles of the permafrost and non-permafrost areas in Alaska. The frequency of junction angles of Mars is more similar to that in the non-permafrost area of Alaska, which suggests that the VNs on Mars were formed by overland flow erosion in non-permafrost area.

The findings from Seybold et al. (2017, 2018) suggest that the frequency of junction angle is less influenced by the post-formational modification processes and can be an indicator of the climatic factors of VNs' formation. In this paper, we compared the associations between the mean junction angles and different environmental factors (climatic and geological factors) on Earth and modeled the associations between the frequency of junction angles and climatic factors (*AI* and *MAP*). We then applied associations between junction angle and *AI* and *MAP* established on Earth to estimate the *AI* of Mars and scaled the estimated *MAP* to account for the different radiation each planet receives from the Sun. Next, we estimated the duration of "warm" Mars by utilizing the minimum cumulative volume of water required to form the VNs (Luo et al., 2017) and the discharge derived from *MAP* (assuming that 1/3 to 1/2 of *MAP* runs off and spreads evenly over the watershed or grid). Our results suggest that the climatic condition of ancient Mars was similar to the arid or semi-arid area on Earth and that the estimated duration of "warm" Mars supports an "episodically warm" Mars.

2. Dataset

For the global Mars VN lines, data from two independent sources were considered. The VN lines of Luo and Stepinski (2009) were automatically extracted utilizing a morphology-based method coupled with flow simulation based on Mars Obiter Laser Altimeter (MOLA) digital elevation model (DEM) data ($\sim$463 m resolution, Smith et al., 2001). The VN lines of Hynek et al. (2010) were manually drawn based primarily on interpretation of Thermal Emission Imaging System (THEMIS) mosaic images ($\sim$230 m resolution, Christensen et al., 2004) and with reference to MOLA data. The VNs from Hynek et al. (2010) contain more details in high valley density areas because the VNs were drawn from higher resolution images. In low density areas, the VNs from Luo and Stepinski (2009) performed better because automatic algorithm was able to extract valleys based on topography that were not obvious on images due to resurfacing processes.

The terrestrial stream data and hydrological units were obtained from the NHDPlusV2 Dataset (McKay et al., 2014). The streams were derived from the several national topographical maps, with spatial scales comparable with the streams extracted from DEM at a resolution of approximately 30 m. For our basic units of analysis or statistical units, we used the HUC-6 (Hydrologic Unit Code-6) watersheds, small grids (158 km by 158 km), and large grids (500 km by 500 km) (see explanation in section 3.3.1).

We used Mean Annual Precipitation (*MAP*) and Aridity Index (*AI*) to represent the long term terrestrial climate. The *AI* is the index of the generalized climate classification which was defined

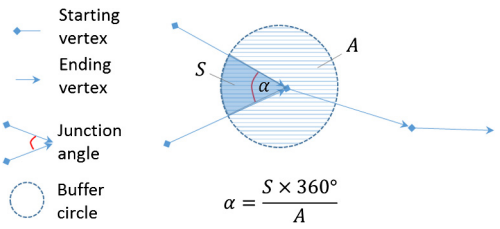

Fig. 1. Diagram illustrating VN junction angle calculation based on VN topology information. (Arrows represent the overall directions of VNs after simplification to remove bias by local topography.)

by the UNEP (1997) and is the ratio of *MAP* and Mean Annual Evaporation (*MAE*). All these three data were based on monthly average data from 1950 to 2000 provided by CGIAR-CSI (Zomer et al., 2007, 2008).

The geological conditions are represented by the surficial lithology and faults. The surficial lithology (Soller et al., 2009), which was based on texture, internal structure, thickness, and environment of deposition is selected to represent the geological factor. Also, some streams, such as those with rectangular drainage pattern, are controlled by the linear geological structure, so we used the faults data to represent the linear structure. The faults data come from the Database of the Geologic Map of North America (Garrity and Soller, 2009). The database includes drainage, geologic units, faults, etc. The database is developed based on the geological map at 1:5,000,000 scale. In the database, there are more than three thousand faults in the conterminous U.S. area.

3. Method and procedure

3.1. Junction angle extraction

The junction angle is the branching angle between two joining stream lines (Fig. 1). We extracted the junction angles by utilizing the topological information of the VNs (or streams) stored in the GIS database. We developed a Python program to extract the junction angle automatically in ArcGIS. The Python code has the following steps. (1) It simplifies the VNs lines (Douglas and Peucker, 1973) to obtain the overall direction of VNs near the intersection points and thus removes the bias by local topography. (2) The program searches all the potential junction points and extracts the simplified VN line segments within the circles (buffers' radius = 10 m) centered on the potential junction points (Fig. 1). The numbers of the starting vertices and ending vertices in each circle are counted; if there are two ending vertices and one starting vertex at the same location, which means that two up-stream VNs merge to a down-stream VN, the center point is a real junction point. (3) The program then calculates the junction angle (α) based the area of the slice formed by the two upstream VNs and the circle (S) and the area of the whole circle (A): $\alpha = (S \times 360°)/A$.

Because the method described above relies on topological information to extract junction angles, accurate topological information in the VN/stream data is critical. Since the VNs from Luo and Stepinski (2009) and streams from NHDPlus v2 are automatically extracted from DEM, their direction follows topography and the topological information is accurate. The VNs from Hynek et al. (2010) are manually drawn from the remotely sensed images, so some VNs' direction may not always follow the topography. To assess the data quality of junction angles, we compared the junction angles obtained from the two datasets in Table 1.

The inconsistency in mean junction angles between the two results is due to the inaccurate topology of some VNs in the manually derived Hynek et al. (2010) data. This is confirmed by the abnormal high frequency of large junction angles and by manual check. The frequency of large angles (greater than 120°) from Hynek et al. (2010) is abnormally high (see Table 1). The range of frequency of junction angles which are greater than 120° is from 6.18% to 9.75% on Earth. Our manual checks also confirmed that some VNs' flow directions of Hynek et al. (2010) are not correct since they are manually digitalized. For this reason, we will only report the result based on the VNs data from Luo and Stepinski (2009) for the rest of the study.

3.2. Spatial association measures by SPADE detector

To compare the associations between junction angle and environmental conditions, we applied the SPatial Association DEtector (SPADE) (Cang and Luo, 2018) to assess the associations. The SPADE is an improvement of the Geo-detector (Wang et al., 2016), which assesses the association by analyzing the variance. The SPADE solved the two main drawbacks of the Geo-detector, which does not consider distance decay and is influenced by the number of discretization zones for continuous variables. After we improve the Geo-detector, the SPADE is a spatial method considering the distance and minimize the influence of discretization so that it is applicable to both continuous and discrete variables. The association is represented by an association parameter usually ranging between 0 and 1, with 0 representing no association and 1 perfect association. The details of SPADE can be found in Cang and Luo (2018).

3.3. Comparative analysis procedure

3.3.1. Terrestrial data analysis

For terrestrial analysis, we selected streams in the conterminous U.S. as our terrestrial data because the conterminous U.S. include varied climates types and have detailed stream information and the geological and climatic database. To compare the influence of climatic and geological factors, we set the mean junction angle as the dependent variable and use the environmental factors (climatic factors: climate types, *AI*, and *MAP* and geologic factors: lithology and density of faults) as the independent variables respectively, then used the SPADE to investigate their associations and ranking.

The dependent variable, mean junction angles, is the averaged junction angles by statistical units, which are HUC-6 (Hydrologic Unit Code-6) watershed, small grids (158 km by 158 km) or large grids (500 km by 500 km). To model the associations between junction angles and climatic factors, we averaged the *AI* and *MAP*

Table 1
Basic statistical result of Mars junction angles.

	Mean of junction angle	No. of junction points	No. of junction angles > 120°	Mean of junction angles < 120°
Luo and Stepinski	58.39°	28,620	848 (≈2.96%)	56.49°
Hynek et al.	68.15°	22,659	2,832 (≈12.63%)	57.38°
All terrestrial (U.S.) data	73.31°	867,804	77,322 (≈8.91%)	66.71°
Terrestrial humid area	76.13°	157,666	15,356 (≈9.74%)	69.23°
Terrestrial arid area	62.91°	178,143	11,005 (≈6.18%)	58.81°

The averaged *AI* by watersheds are classified to five classed by the quantile classification method. The humid area is the watersheds whose *AI* are greater than 1.034. The arid areas' *AI* are smaller than 0.382.

by the same statistical units as the dependent variables. To assess the associations between junction angles and geological factors, we used zonal majority of surficial lithology by the zones of same statistical units and calculated density (m/km^2) of faults (representing the power of linear geological structure) by the same statistical units as the dependent variables. Since the control of geologic structure on streams is often reflected in the rectangular drainage pattern with mostly right junction angles, we also used the ratio of right junction angle in statistical units to represent the junction angle.

For the statistical unit, we used not only the HUC-6 watersheds, but also square grids (with each grid area equaling to the mean area of the HUC-6 or equaling to the grids used on Mars data) to process our data. The watershed boundaries on Mars are often poorly defined due to the influence of impact cratering and the low density of VNs on Mars, so it is desirable to use a simple unit such as square grid. To obtain enough junction angles in each grid, the size of statistic unit on Mars is assigned as 500 km by 500 km. To compare the difference between the different sizes and shapes, we chose all the three statistical units for the measures of terrestrial association and estimates of Mars climatic conditions.

3.3.2. Terrestrial data modeling

For the purpose of applying the associations between climatic factors and junction angles to Mars, we used the Ordinary Least Squares (OLS) regression and k-NN regression (k-nearest neighbor regression) to model to the associations between the climatic factors and the frequency of junction angles.

We selected the OLS regression because the previous research (Seybold et al., 2017, 2018) indicated that the association between the logarithmic *AI* and junction angles may be close to linear, but Seybold et al. (2017, 2018) did not prove that. To consider the possibility that the association between junction angles and climatic factors is nonlinear, we applied k-NN regression to model the association between the frequency of junction angle and environmental factors. The OLS regression and the k-NN regression are implemented by Pedregosa et al. (2011).

The dependent variables in the regression, or the training data in the k-NN regression, are the logarithmic climatic factors (*AI* and *MAP*) and the independent variables are the frequencies of junction angle in bins (bin $= 10°$). The reason for selecting frequency distribution of junction angle, as opposed to the mean junction angles, is that the frequency distribution contains more information than the simple mean. The modeled associations were utilized in the section 3.3.3 to estimate the *AI* and *MAP* of the Noachian Mars.

3.3.3. Inferring Mars climatic conditions

We first compared the junction angles on Mars and Earth. The comparisons are made between the frequency distribution of all junction angles considered on Mars surface (hereafter simply referred to as global Mars) and frequency distributions of junction angles in the conterminous U.S. We used quantile classification method to group the HUC-6 watersheds to five groups based on their *AI*s. Then we calculated the frequency distribution of junction angles in each group and compared them with frequency distribution of Mars junction angle.

We also applied the model results from the OLS regression and k-NN regression obtained on Earth to the global frequency distribution of Mars junction angles to estimate the global *AI* and *MAP* of Mars. Note, because the radiation each planet received from the Sun is different, the estimated *MAP* from the model does not represent the *MAP* on the Noachian Mars. To obtain the *MAP* on the Noachian Mars, we need to consider the difference in solar radiation each planet receives from the Sun, which can be calculated as the ratio of *MAE* between the Mars and Earth. This ratio is then used to scale the *MAP* estimated from the model. The scale processing is described in section 3.3.4.

To consider the spatial distribution of climate on Noachian Mars, we divided the entire Mars surface to grids, each with size of 500 km by 500 km, which can be considered a climatically homogeneous area. We selected the grids within denser junction angle belt for analysis. After we grouped the junction angles to each grid, we extracted the frequencies of junction angles in each grid and applied the OLS regression and k-NN regression models derived from terrestrial data, to estimate the *AI* and *MAP* of each grid on Mars. Similar to global frequency analysis, we also used the ratio of *MAE* between the Mars and Earth to scale the estimated *MAP* of each grid on the Noachian Mars.

3.3.4. Estimating the duration of "warm" Mars

To consider the difference in solar radiation Earth and Mars received from the Sun, we use the Potential Evaporation (*PE*) to represent the *MAE*. The replacement is also used in the Earth climatic data production (Zomer et al., 2007, 2008). The *PE* on Earth can be related to radiation by Hargreaves evapotranspiration equation (Hargreaves and Allen, 2003) as follows:

$$PE = 0.0023^{*}RA^{*}(T_{mean} + 17.8)^{*}TD^{0.5}\ \text{mm/month} \quad (1)$$

where T_{mean} is mean temperature; *TD* represents daily temperature range; and *RA* is radiation received from the Sun.

Due to the faint young Sun and the distance between Mars and the Sun, Mars only receives 1/3 of solar radiation that Earth receives. The mean temperature and daily range have more uncertainty. At the lower end, we assume $T_{mean} = 0\,°\text{C}$ and $TD = 22.2\,°\text{C}$ (same as terrestrial value), which will make Mars *PE* about 1/5 of terrestrial value. At the upper end, we assume $T_{mean} = 9.75\,°\text{C}$ (Wordsworth et al., 2015) and $TD = 60\,°\text{C}$ (based on Viking record (Lewis et al., 1999)), which would give Martian *PE* about 1/2 of terrestrial value. We assume these same ratios in *PE* estimates also apply to *MAP* estimates when *AI*s are the same.

Next, we utilized the frequency of junction angles of global VNs to estimate the duration of "warm" Mars. We divided volume of water required to form the VNs (Luo et al., 2017) by the discharge (assuming that 1/3 to 1/2 of *MAP* runs off and spreads evenly over grid) to obtain the VNs' formation timescale. To estimate the duration of the "warm" Mars, we adopted a 1% intermittence because our estimated the *AI* of Noachian Mars falls in the zone of semi-arid or arid, for which the intermittence is 1% (Orofino et al., 2018).

To infer local/regional climate at grid level, we only selected the upstream grids (shown as hatched areas in Fig. 2) to estimate the duration of "warm" Mars to avoid the complication that water flowed in the downstream grids were not only from the precipitation, but also from upstream areas.

4. Results

4.1. Terrestrial junction angle analysis

There are a total of 867,804 junction angles extracted from the conterminous U.S. The mean and standard deviation of the junction angle are 73.31°, 32.98° respectively. The associations between the junction angles and the environmental factors using SPADE are shown in Table 2(a). The associations between the linear geological structure and the junction angles using SPADE are in Table 2(b).

In Table 2(a), the influences of climatic types and lithology vary under different size and shape of statistical units. Although we cannot prove which one is more important, we find that the lithology and climatic types both have significant influence on the junction angles, and influence of climatic types is stronger than or at

Table 2
Associations using SPADE (larger value means higher association).
a. Association between mean junction angles and environmental factors on Earth

		Lithology	Density of faults	Climate types	Aridity index	Mean annual precipitation
Mean junction angle	HUC-6	0.33	0.14	0.38	0.46	0.39
	158 km × 158 km	0.41	0.15	0.39	0.53	0.47
	500 km × 500 km	0.27	0.06	0.26	0.63	0.38

b. Associations between density of faults and junction angle and between density of faults and ratio of right angles

		Mean junction angle	Ratio of right junction angle
Density of faults	HUC-6	0.08	0.14
	158 km × 158 km	0.07	0.09
	500 km × 500 km	−0.03	0.02

Table 3
Model performance on terrestrial data.
a. Model based on the HUC-6

	OLS	k-NN ($k=1$)	k-NN ($k=10$)	k-NN ($k=50$)
log(*AI*)	0.59	1.0	0.67	0.57
Log(*MAP*)	0.49	1.0	0.61	0.48

b. Model based on the grids with size of 158 km × 158 km

	OLS	k-NN ($k=1$)	k-NN ($k=10$)	k-NN ($k=50$)
log(*AI*)	0.65	1.0	0.69	0.62
Log(*MAP*)	0.55	1.0	0.62	0.53

c. Model based on the grids with size of 500 km × 500 km

	OLS	k-NN ($k=1$)	k-NN ($k=3$)	k-NN ($k=5$)
log(*AI*)	0.82	1.0	0.86	0.80
Log(*MAP*)	0.74	1.0	0.75	0.66

least on a par with the influence of lithology; so the climatic influence cannot be ignored. The results in Table 2(b) showed that the associations between the linear geologic structures (faults) and the junction angles are weak at the conterminous U.S. scale. Although the linear structures can influence the junction angles at the fine scales and form the rectangular drainage pattern, the influence from the surficial lithology is a majority factor at the conterminous U.S. scale, so we do not consider the linear structure as an influence factor in this research. Based on this result, we confirmed that the junction angles are influenced by the surficial lithology and climatic factors. Since this research focuses on the influence of water to the junction angles, we investigated the association between the junction angles and *AI* and *MAP*. Their associations are stronger than the lithology and climatic types, which means that *AI* and *MAP* are more predictable by the junction angles.

Table 3 shows the performance scores of OLS regression and k-NN regression models (higher score representing better performance). To ensure the robustness of the modeling results, we assigned $k = 1, 10$, and 50 for HUC-6 watershed and grids with size of 158 km by 158 km and assigned $k = 1, 3$, and 5 for grids with size of 500 km by 500 km because the total number of grids in this large size is 47, which is much fewer than the number of small grids (more than 300). Most scores are greater than 0.6. In the k-NN regression, the model scores, when k is small, are greater than the OLS regression model although it may have some overfitting risks. The model scores of k-NN regression decrease with the increase of k values. When the k is large enough (such as $k = 50$ for the small statistical units or $k = 5$ for the large statistical units), the scores of k-NN regression are smaller than the scores of OLS regressions.

The scores from the grids with size of 500 km by 500 km are larger than the scores from other statistical units, because the large grids may group more details together. However, it does not mean that the large grids are much better than other smaller statistical units due to the complexity of spatial self-organization and spatial

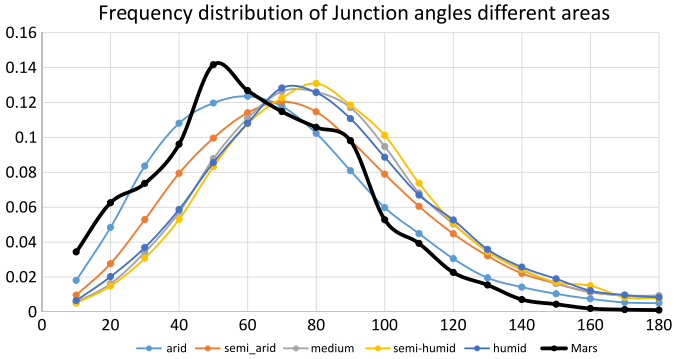

Fig. 2. Frequency distribution of junction angles on the global and in different terrestrial zones of Earth. (For interpretation of the colors in the figure(s), the reader is referred to the web version of this article.)

scale. For example, if the all junction angles are grouped to one group, the model score is 1 (high score, but meaningless). We did not compare which model is the best in detail. We chose the three statistical units and took advantage of the OLS regression model and the k-NN regression models excluding the large k to estimate the climatic condition of Mars.

4.2. Global and local Mars VNs analysis

Based on the terrestrial junction angle analysis, the frequency distribution of junction angles acts as an indicator of the long-term climate. We extracted the global junction angles of Mars and plotted the frequency distribution of global Mars junction angles and terrestrial junction angles (statistical unit: HUC-6) together. Fig. 2 shows that the frequency distribution of global Mars junction angles is generally between the arid ($AI < 0.38$) and semi-arid ($0.38 < AI < 0.68$) areas in the conterminous U.S. It indicates that climate of ancient Mars was wetter than the driest areas of U.S.

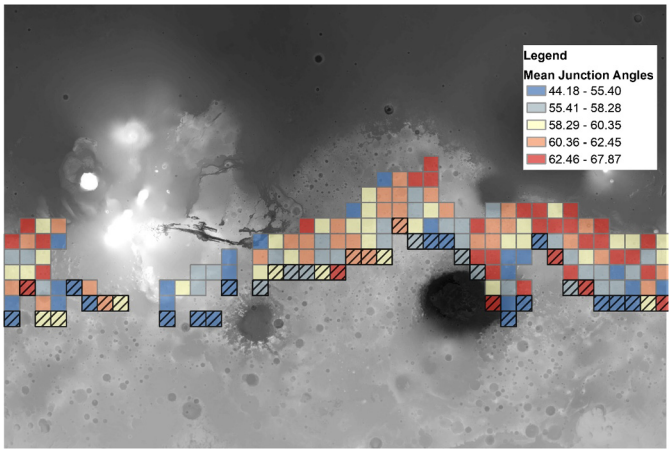

Fig. 3. Spatial distribution of estimated junction angle of Mars. The hatched grids are the upstream grid.

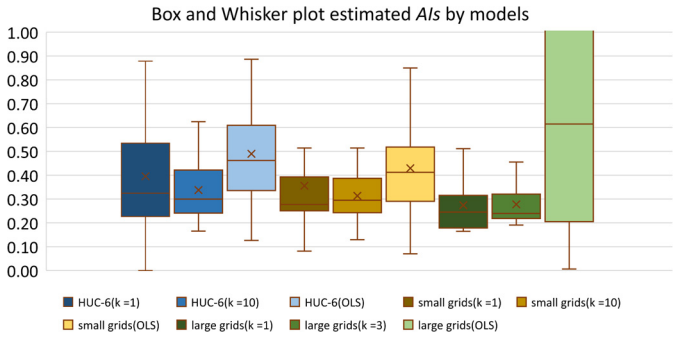

Fig. 4. Box and whisker chart of the estimated *AI* of Noachian Mars by models. The bottom and top of box represent first quartile and third quartile. The median is represented by line in the box. The mean is denoted by the "X" marker. Followed the Tukey industry standard, the maximum length form whisker to its nearest box is 1.5 times the length of the box. The box and whisker of large grids (OLS) includes too many outliers, so a part of the box is shown.

To analyze the spatial distribution of estimated climatic conditions, we divided the entire Mars surface to square grids of 500 km by 500 km and then calculated the frequency of junction angels within each grid and estimated *AI* of each grid. To minimize the influence of post-formation process, we only select the grids located in the dense VNs belt (Fig. 3).

The spatial distribution of mean junction angles of each grid is shown in Fig. 3. The general trend is that the junction angles in the north are larger than those in the south, which indicates that the northern areas were wetter than the southern areas (Seybold et al., 2017).

We also analyzed the spatial distribution of estimated *AI* by calculating the association between *AI* and coordinates (latitude and longitude) of grid centers. To avoid the influence of non-linear association between variables, we chose Spearman's rank correlation coefficient (Spearman's rho) which assumes that a perfect monotone function reaches the highest correlation ($+1$ or -1) if there are no repeated data values. The Spearman's rho between the junction angles and the latitude (to make interpretation easier, the latitude of north pole is defined as 0° and south pole 180°) is -0.37 (see also Table 5(a)), and the associations between the junction angles and the longitude is not significant.

4.3. Estimated climatic conditions and duration of "warm" period

We applied the association between junction angle and *AI* learnt from the OLS regression and *k*-NN regression models on Earth to estimate the *AI* of the ancient Mars. Using the global frequency of junction angles of Mars, the range of estimated *AI* from different models is from 0.18 to 0.47, the median and mean are 0.35 and 0.32, respectively. We also applied the associations to the junction angles grouped by grids, and the statistics of the results based on grids are shown in Fig. 4.

After we estimated the *MAP* of the global Mars by utilizing the terrestrial models and scaled *MAP* based on the estimated ratio of *MAE* between Earth and Mars, we calculated the formation timescale of VNs by dividing the minimum volume of water required (Luo et al., 2017) by discharge derived from *MAP* (assuming that 1/2 to 1/3 of scaled *MAP* runs off and spreads evenly over the area of the grids analyzed, in m^3/yr). Then, we divided the formation time scale by 1% (intermittence) to obtain the "warm" period duration. The results are shown in Table 4. We excluded the results from OLS regression (large grids). The reason is described in the section 5.1. The range of "warm" period duration is from 7.8(4) to 77.(05) million years.

We also estimated and scaled the local *MAP* by utilizing the frequency of junction angles and the terrestrial models. To avoid the complication that downstream areas receive water from precipitation and contribution from upstream and the fact that VNs at lower elevation are more likely influenced by non-fluvial processes, we only considered upstream grids (shown as hatched areas in Fig. 3). Then, we calculated the mean "warm" period duration as the results, which are shown in Table 4. The duration of "warm" period is from 4.4(3) $\sim$ 34.(81) million years.

5. Discussion and conclusion

5.1. Terrestrial models selection

We excluded the results from OLS model (large grids), because the estimated Mars climatic conditions from this model are abnormal and with many outliers. The estimated *AI* and the duration of "warm" Mars are much greater than the results from other models. Some grids' (12 of 39 upstream grids) have *AI* values greater than 1.5. Recall that *AI* is the ratio between precipitation and potential evapotranspiration, a value of 1.5 means that precipitation is 1.5 times of *PE*, a very humid condition, which were unlikely for Mars. Meanwhile, the results have the highest *AI* and the long duration at the same time, which are likely caused by the outliers. Usually, the higher the *AI*, the higher the *MAP*; and the higher *MAP* will result in the shorter formation timescale. In the other two statistical units, the estimated *AI*s from OLS regression are larger than the *AI*s from *k*-NN regression and the estimated formation timescales from OLS regression are shorter. This shows that the size relationship between the estimated *AI* and timescale is self-consistent.

5.2. Estimated Mars climatic conditions

The estimates of the Mars *AI* are consistent with previous research results by Matsubara et al. (2011 and 2013). Matsubara et al. (2011 and 2013) used the *X*-ratio to express climatic conditions. Landform simulation modeling has established that the range of *X*-ratio is from 1 to 7 (Matsubara et al., 2011, 2013). The *X*-ratio is defined as

$$X = \frac{E - P}{P R_B} \tag{2}$$

where E is evaporation; P is precipitation; R_B is the fraction of precipitation that contributes to runoff. Higher *X*-ratio represents drier climate.

Based on the definition of *X*-ratio and *AI*, the two can be related to *AI* by the following equation:

$$AI = \frac{1}{1 + X R_B} \tag{3}$$

Table 4
Estimated duration of "warm" Mars (unit: million years).

		HUC-6			158 km*158 km			500 km*500 km		
		OLS	KNN_1	KNN_10	OLS	KNN_1	KNN_10	OLS	KNN_1	KNN_3
Global JA	LL	7.8(4)	13.(84)	13.(42)	9.0(1)	15.(33)	13.(07)	3.4(7)	18.(49)	13.(86)
	UL	32.(68)	57.(67)	55.(90)	37.(53)	63.(89)	54.(45)	14.(45)	77.(05)	57.(76)
Up stream JA	LL	4.4(3)	7.4(1)	7.3(8)	5.7(2)	7.4(5)	7.8(9)	69.(39)	8.3(5)	7.9(2)
	UL	18.(45)	30.(87)	30.(77)	23.(84)	31.(02)	32.(88)	28(9.13)	34.(81)	33.(00)

LL = lower limit; UL = upper limit; JA = junction angle. The gray numbers are excluded due to the too many outliers from this model.

Table 5
Spatial analysis of landform characteristics and estimated *AI*.

a. Spearman's rho matrix of landform characteristics

	Mean junction angle	Mean elevation	Latitude (0 N pole ~ 180°S pole)	Minimum water volume required to form VNs
Mean junction angle	–	–	–	–
Mean elevation	−0.24**	–	–	–
Latitude (0 N pole ~ 180°S pole)	−0.37***	0.32***	–	–
Minimum water volume required to form VNs	0.29***	−0.34***	−0.39***	–

b. Correlation between *AI* estimated by different models and landform characteristics

	HUC-6			158 km*158 km			500 km*500 km	
	OLS	KNN_1	KNN_10	OLS	KNN_1	KNN_10	KNN_1	KNN_3
Latitude (0 N pole~180°S pole)	−0.25***	−0.30***	−0.40***	−0.31***	−0.03 (ns)	−0.35***	−0.42***	−0.43***
Mean elevation	−0.12 (ns)	−0.22**	−0.25***	−0.07 (ns)	−0.10 (ns)	−0.21**	−0.20**	−0.25**
Minimum water volume required to form VNs	0.20**	0.16*	0.24**	0.20**	0.26***	0.20**	0.21**	0.25**

ns: $P > 0.05$; *: $P \leq 0.05$; **: $P \leq 0.01$; ***: $P \leq 0.001$.

The range of R_B is from 0 to 1, so the range of *AI* is from 0.125 to 1 (considering X-ratio ranges from 1 to 7). In our research, we assume the range of R_B is from 0.33 to 0.50. Following our assumption, the range of equivalent *AI* is from 0.22 to 0.75. The estimated global *AI*s, which is calculated from the frequency distribution of global junction angle, is within this range.

Seybold et al. (2018) revealed that the climatic condition of Noachian Mars was similar to the MDRS because they have similar drainage patterns, suggesting that the basin and its surroundings are similar to Martian landscape and that's why it is selected as an analog location to train astronauts. The MDRS is located at the Upper Colorado-Dirty Devil basin (HUC 1407). The mean *AI* of HUC 1407 watershed is 0.20 (Zomer et al., 2007, 2008). The minimum, median and maximum *AI* estimated by the global frequency of junction angles of Mars is 0.18, 0.32 and 0.46, respectively. The *AI* of HUC 1407 watershed is within the range of our estimated *AI*. Although our estimated *AI*s are a little bit greater than the *AI* of HUC 1407 watershed, the HUC 1407 watershed was wetter during the late Pleistocene (Matsubara and Howard, 2009; Matsubara et al., 2011, 2013) when the landform of HUC 1407 watershed formed. The similar *AI*s showed that our estimated results are reasonable.

The spatial pattern of estimated *AI*s also supports that our estimated conditions are reasonable. No matter whether ancient Mars was "warm" or "cold", the liquid water flowed on the surface of Mars (Wordsworth et al., 2018) in the Noachian period and accumulated in the northern basin. To test the hypothesis of Wordsworth et al. (2018), we calculated the Spearman's Rho matrix of landform characteristics (mean junction angle, mean elevation, latitude, minimum water volume required to form VNs) (Table 5(a)). The results suggest that the lower the elevation and the farther north one goes, the larger the junction angle and the more the water required to carve the VNs, which is consistent with the scenario of an integrated hydrologic cycle with water flowing from south to north. In this case, the northern area should have more water due to the accumulative effect. If this hypothesis is correct, the estimated *AI*s should have positive correlation with the volume of required water to form VNs and have negative correlation with the distance of grid to north pole. To test whether the spatial distribution of our estimated *AI*s is consistent with the spatial distribution of volume of required water to form VNs, we calculate the Spearman's Rho between the estimated *AI* and center latitude, mean elevation, and volume of required water to form VNs by grid, respectively. The results are showed in Table 5(b).

In Table 5(b), the estimated *AI*s have significant positive correlation with the volume of water required to form VNs (Luo et al., 2017) across all models, consistent with wetter area supplying more water for erosion processes. Also, most estimated *AI*s have significant negative correlation with the latitudes (the values of latitude from north pole to south pole is defined as 0~180°). This shows that the northern areas are wetter than the southern areas.

Since more fluvial erosion needs more water, our estimated *AI*s, derived from junction angle frequencies, are consistent with the volume of water required to form VNs, independently derived from DEM (Luo et al., 2017). Both the values of estimated *AI*s and the volume of water required to form VNs decrease from northern basin to southern highland. It indicates that the water flowed from southern highland to northern basin and accumulated more water downstream. The trend supports the hypothesis that the Mars had a global hydrological cycle and the surface water flowed from southern highland to the northern basin. This consistency indicates that the spatial trend of our estimated *AI* is reasonable.

5.3. Estimated duration of "warm" Mars

Our estimated duration of "warm" period using all VNs (with an upper limit of around 77 million years) is longer than the duration using upstream areas only (4.4(3) to 34.(81) million years). Because VNs at lower elevation are more likely to be influenced by non-fluvial processes, we prefer the estimate of duration using upstream grids (4.4(3) to 34.(81) million years). It is important to note that our estimated length of "warm" period was obtained by integrating the climatic model and the geomorphological evidence. The estimated duration using all VNs and estimated duration using only upstream VNs have the same order of magnitude, but the former is usually larger than the latter by a factor of two.

The intermittence values depend on the aridity of Mars. If the Mars climatic condition was hyper-arid, the intermittence value is 0.1% (Orofino et al., 2018); if the Mars was semiarid/arid, the intermittence value is 1% (Orofino et al., 2018); and if Mars climatic condition was humid/sub-humid, the intermittence is 5% (Hoke et al., 2011). We took the intermittence value for semiarid/arid for Mars, because the range of our estimated *AI*s falls between the zones of arid and sub-arid. Moreover, previous research relating the climate condition of Noachian Mars (Seybold et al., 2018; Matsubara et al., 2011, 2013) have the same or similar conclusion.

The duration of "warm" Mars is also estimated by other researchers. Hoke et al. (2011) applied Darcy–Weisbach equation and sediment transport models to the landform characteristics of large VNs to estimate the formation timescale. In Hoke et al. (2011)'s research, the concept of intermittence formation timescale is similar to the duration of "warm" Mars in our paper. The typical range of intermittence formation timescale of Hoke et al. (2011) is between 0.1 and 100 million years. The range of our estimated duration of "warm" Mars is consistent with their results, but we have a narrower range.

Orofino et al. (2018) took advantage of modified Manning's equation and the VNs' landform characteristics to estimate the discharge. They then divided the volume of water required by the estimated discharge to estimate the possible range of water flow duration, which is considered as the duration of "warm" Mars in our paper. The range of water flow duration is 0.01 to 200 million years (median is 0.5 million years). Our results are within this range and is better constrained to a narrower range.

5.4. Additional uncertainties from channel bed conditions and orbital obliquity

The volume of water required to form the VNs was the minimum cumulative volume globally (Luo et al., 2017). Thus the duration of the erosion we estimated in this study should also be considered the lower bound. In addition, if the VNs beds are floored by coarse gravels/boulders or armored by coarse sediment (Howard et al., 2016) or at least locally composed of bedrock, erosion rates could be dramatically slower (Sklar and Dietrich, 2001, 2004) and the formation duration could be significantly longer than our results in Table 4.

In addition, since the climate of Mars was controlled by obliquity variation, the "warm" Mars might only occur a small fraction of the time during the obliquity cycles (Mischna et al., 2013). If this hypothesis is correct, the obliquity cycle gave an additional intermittency on top of the intermittency of runoff events. The total duration of VNs' formation (from the first to the last runoff incisions of VNs) could have been dramatically longer than even the least conservative published estimates, but the effective incision duration would still be similar to our estimates.

5.5. Conclusion

Stream/VN junction angles offer an important means to uncover processes and climate that formed the streams/VNs, because the angles and their spatial and frequency distribution contain fingerprints left by these processes and climatic conditions. Furthermore, the junction angle is a robust property that is minimally influenced by post formational modification processes.

Our terrestrial analysis in the conterminous U.S. confirmed that surficial environmental factors (lithology and climate type) significantly correlated with the junction angles and that the *AI* and *MAP* can be predicted by frequency of junction angles. The frequency of global junctions on Mars allows us to estimate the climatic condition (*AI* and *MAP*) of the Noachian Mars. The range of estimated *AI*s using all junction angles is from 0.18 to 0.47, which is consistent with previous research using other landform characteristics. The duration of "warm" Mars can be estimated by the discharge derived from scaled *MAP* and water volume required to form VNs. The range of estimated duration of "warm" Mars using all junction angles is from 7.8(4) to 77.(05) million years; the range of estimated duration of "warm" Mars using upstream junction angles is from 4.4(3) to 34.(81) million years. Although the estimates using all VNs are larger than the estimates using upstream VNs by about a factor of two, they are in the same order of magnitude.

With junction angle as a robust and reliable property that reflects past climate and processes as shown in our terrestrial analysis, we are confident with our interpretation of the junction angle frequency on Mars. The global junction angles frequency on Mars supports that the *AI* of Noachian Mars is similar to those of the arid/sub-arid regions on Earth. The correlation with water volume required to form VN and latitude results suggest that our estimated climatic conditions are consistent with the scenario of an integrated hydrologic cycle that water flows from south to north. It is important to note that our estimated length of "warm" period was obtained by integrating the climatic model and the geomorphological evidence, although it should be considered the lower bound due to uncertainties in channel bed conditions and orbital obliquity. Considering the Noachian period is 400 million years, both results support the hypothesis that Mars was "episodically warm."

Acknowledgement

We thank two anonymous reviewers for their helpful comments.

References

Baker, V.R., Hamilton, C.W., Burr, D.M., Gulick, V.C., Komatsu, G., Luo, W., Rice Jr., J.W., Rodriguez, J.A.P., 2015. Fluvial geomorphology on Earth-like planetary surfaces: a review. Geomorphology 245, 149–182.

Cang, X., Luo, W., 2018. Spatial association detector (SPADE). Int. J. Geogr. Inf. Sci. 32 (10), 2055–2075.

Christensen, P.R., Jakosky, B.M., Kieffer, H.H., Malin, M.C., McSween, H.Y., Nealson, K., Mehall, G.L., Silverman, S.H., Ferry, S., Caplinger, M., Ravine, M., 2004. The thermal emission imaging system (THEMIS) for the Mars 2001 Odyssey mission. Space Sci. Rev. 110 (1–2), 85–130.

Craddock, R.A., Howard, A.D., 2002. The case for rainfall on a warm, wet early Mars. J. Geophys. Res., Planets 107 (E11).

Davis, J.M., Balme, M., Grindrod, P.M., Williams, R.M.E., Gupta, S., 2016. Extensive Noachian fluvial systems in Arabia Terra: implications for early Martian climate. Geology 44 (10), 847–850.

Di Achille, G., Hynek, B.M., 2010. Ancient ocean on Mars supported by global distribution of deltas and valleys. Nat. Geosci. 3 (7), 459.

Douglas, D.H., Peucker, T.K., 1973. Algorithms for the reduction of the number of points required to represent a digitized line or its caricature. Cartographica: Int. J. Geogr. Inf. Geovis. 10 (2), 112–122.

Ehlmann, B.L., Mustard, J.F., Murchie, S.L., Bibring, J.P., Meunier, A., Fraeman, A.A., Langevin, Y., 2011. Subsurface water and clay mineral formation during the early history of Mars. Nature 479 (7371), 53.

Garrity, Christopher, Soller, David, 2009. Database of the Geologic Map of North America. Adapted from the Map by J.C. Reed Jr. and others.

Gough, D.O., 1981. Solar interior structure and luminosity variations. In: Physics of Solar Variations. Springer, Dordrecht, pp. 21–34.

Gulick, V.C., 1998. Magmatic intrusions and a hydrothermal origin for fluvial valleys on Mars. J. Geophys. Res., Planets 103 (E8), 19365–19387.

Halevy, I., Head III, J.W., 2014. Episodic warming of early Mars by punctuated volcanism. Nat. Geosci. 7 (12), 865.

Hargreaves, G.H., Allen, R.G., 2003. History and evaluation of Hargreaves evapotranspiration equation. J. Irrig. Drain. Eng. 129 (1), 53–63.

Hoke, M.R., Hynek, B.M., Tucker, G.E., 2011. Formation timescales of large Martian valley networks. Earth Planet. Sci. Lett. 312 (1–2), 1–12.

Hooshyar, M., Singh, A., Wang, D., 2017. Hydrologic controls on junction angle of river networks. Water Resour. Res. 53 (5), 4073–4083.

Horton, R.E., 1932. Drainage-basin characteristics. Eos 13 (1), 350–361.

Horton, R.E., 1945. Erosional development of streams and their drainage basins; hydrophysical approach to quantitative morphology. Geol. Soc. Am. Bull. 56 (3), 275–370.

Howard, A.D., Breton, S., Moore, J.M., 2016. Formation of gravel pavements during fluvial erosion as an explanation for persistence of ancient cratered terrain on Titan and Mars. Icarus 270, 100–113.
Hynek, B.M., Phillips, R.J., 2003. New data reveal mature, integrated drainage systems on Mars indicative of past precipitation. Geology 31 (9), 757–760.
Hynek, B.M., Beach, M., Hoke, M.R., 2010. Updated global map of Martian valley networks and implications for climate and hydrologic processes. J. Geophys. Res., Planets 115 (E9).
Lewis, S.R., Collins, M., Read, P.L., Forget, F., Hourdin, F., Fournier, R., Hourdin, C., Talagrand, O., Huot, J.P., 1999. A climate database for Mars. J. Geophys. Res., Planets 104 (E10), 24177–24194.
Luo, W., Stepinski, T.F., 2009. Computer-generated global map of valley networks on Mars. J. Geophys. Res., Planets 114 (E11).
Luo, W., Cang, X., Howard, A.D., 2017. New Martian valley network volume estimate consistent with ancient ocean and warm and wet climate. Nat. Commun. 8, 15766.
Matsubara, Y., Howard, A.D., 2009. A spatially explicit model of runoff, evaporation, and lake extent: application to modern and late Pleistocene lakes in the Great Basin region, western United States. Water Resour. Res. 45 (6).
Matsubara, Y., Howard, A.D., Drummond, S.A., 2011. Hydrology of early Mars: lake basins. J. Geophys. Res., Planets 116 (E4).
Matsubara, Y., Howard, A.D., Gochenour, J.P., 2013. Hydrology of early Mars: valley network incision. J. Geophys. Res., Planets 118 (6), 1365–1387.
McKay, L., Bondelid, T., Dewald, T., Rea, A., Moore, R., Johnston, J., 2014. NHDPlus version 2: user guide. Available at http://www.horizon-systems.com/NHDPlus/.
Mischna, M.A., Baker, V., Milliken, R., Richardson, M., Lee, C., 2013. Effects of obliquity and water vapor/trace gas greenhouses in the early martian climate. J. Geophys. Res., Planets 118 (3), 560–576.
Orofino, V., Alemanno, G., Di Achille, G., Mancarella, F., 2018. Estimate of the water flow duration in large Martian fluvial systems. Planet. Space Sci. 163, 83–96.
Pedregosa, F., Varoquaux, G., Gramfort, A., Michel, V., Thirion, B., Grisel, O., Blondel, M., Prettenhofer, P., Weiss, R., Dubourg, V., Vanderplas, J., 2011. Scikit-learn: machine learning in Python. J. Mach. Learn. Res. 12, 2825–2830.
Penido, J.C., Fassett, C.I., Som, S.M., 2013. Scaling relationships and concavity of small valley networks on Mars. Planet. Space Sci. 75, 105–116.
Perron, J.T., Richardson, P.W., Ferrier, K.L., Lapôtre, M., 2012. The root of branching river networks. Nature 492 (7427), 100.
Pieri, D.C., 1980. Martian valleys: morphology, distribution, age, and origin. Science 210 (4472), 895–897.
Ramirez, R.M., Craddock, R.A., 2018. The geological and climatological case for a warmer and wetter early Mars. Nat. Geosci. 11 (4), 230.
Rodriguez, J.A.P., Fairén, A.G., Tanaka, K.L., Zarroca, M., Linares, R., Platz, T., Komatsu, G., Miyamoto, H., Kargel, J.S., Yan, J., Gulick, V., 2016. Tsunami waves extensively resurfaced the shorelines of an early Martian ocean. Sci. Rep. 6, 25106.
Rosenberg, E.N., Palumbo, A.M., Cassanelli, J.P., Head, J.W., Weiss, D.K., 2019. The volume of water required to carve the martian valley networks: improved constraints using updated methods. Icarus 317, 379–387.
Seybold, H., Rothman, D.H., Kirchner, J.W., 2017. Climate's watermark in the geometry of stream networks. Geophys. Res. Lett. 44 (5), 2272–2280.
Seybold, H.J., Kite, E., Kirchner, J.W., 2018. Branching geometry of valley networks on Mars and Earth and its implications for early Martian climate. Sci. Adv. 4 (6), eaar6692.
Sklar, L.S., Dietrich, W.E., 2001. Sediment and rock strength controls on river incision into bedrock. Geology 29 (12), 1087–1090.
Sklar, L.S., Dietrich, W.E., 2004. A mechanistic model for river incision into bedrock by saltating bed load. Water Resour. Res. 40 (6).
Smith, D.E., Zuber, M.T., Frey, H.V., Garvin, J.B., Head, J.W., Muhleman, D.O., Pettengill, G.H., Phillips, R.J., Solomon, S.C., Zwally, H.J., Banerdt, W.B., 2001. Mars Orbiter Laser Altimeter: experiment summary after the first year of global mapping of Mars. J. Geophys. Res., Planets 106 (E10), 23689–23722.
Soller, D.R., Reheis, M.C., Garrity, C.P., Van Sistine, D.R., 2009. Map database for surficial materials in the conterminous United States. US Geol. Surv. Data Ser. 425.
UNEP (United Nations Environment Programme), 1997. World Atlas of Desertification, 2nd ed. UNEP, London.
Wang, J.F., Zhang, T.L., Fu, B.J., 2016. A measure of spatial stratified heterogeneity. Ecol. Indic. 67, 250–256.
Williams, R.M., Phillips, R.J., 2001. Morphometric measurements of Martian valley networks from Mars Orbiter Laser Altimeter (MOLA) data. J. Geophys. Res., Planets 106 (E10), 23737–23751.
Wordsworth, R., Ehlmann, B., Forget, F., Haberle, R., Head, J., Kerber, L., 2018. Healthy debate on early Mars. Nat. Geosci. 11, 888. https://doi.org/10.1038/s41561-018-0267-5.
Wordsworth, R.D., 2016. The climate of early Mars. Annu. Rev. Earth Planet. Sci. 44, 381–408.
Wordsworth, R.D., Kerber, L., Pierrehumbert, R.T., Forget, F., Head, J.W., 2015. Comparison of "warm and wet" and "cold and icy" scenarios for early Mars in a 3-D climate model. J. Geophys. Res., Planets 120 (6), 1201–1219.
Zomer, R.J., Bossio, D.A., Trabucco, A., Yuanjie, L., Gupta, D.C., Singh, V.P., 2007. Trees and Water: Smallholder Agroforestry on Irrigated Lands in Northern India. IWMI Research Report 122. International Water Management Institute, Colombo, Sri Lanka, p. 45.
Zomer, R.J., Trabucco, A., Bossio, D.A., van Straaten, O., Verchot, L.V., 2008. Climate change mitigation: a spatial analysis of global land suitability for clean development mechanism afforestation and reforestation. Agric. Ecosyst. Environ. 126, 67–80.